### Title

Enzymatic Mechanism of Leishmania major Peroxidase and the Critical Role of Specific Ionic Interactions.




### Journal

Biochemistry, 54(21)



### Authors

Chreifi, Georges
Hollingsworth, Scott
Tripathi, Sarvind
et al.



### Publication Date

2015-06-02

### DOI

10.1021/acs.biochem.5b00338

Peer reviewed

Published in final edited form as:

*Biochemistry*. 2015 June 2; 54(21): 3328–3336. doi:10.1021/acs.biochem.5b00338.

# Enzymatic Mechanism of *Leishmania major* Peroxidase and the Critical Role of Specific Ionic Interactions

**Georges Chreifi**[†], **Scott A. Hollingsworth**[†], **Huiying Li**[†], **Sarvind Tripathi**[†,‖], **Anton P. Arce**[†], **Hugo I. Magaña-Garcia**[†], and **Thomas L. Poulos**[*,†,‡,§]

[†]Department of Molecular Biology and Biochemistry, University of California, Irvine, California 92697-3900, United States

[‡]Department of Chemistry, University of California, Irvine, California 92697-3900, United States

[§]Department of Pharmaceutical Sciences, University of California, Irvine, California 92697-3900, United States

## Abstract

*Leishmania major* peroxidase (LmP) is very similar to the well-known yeast cytochrome *c* peroxidase (CcP). Both enzymes catalyze the peroxidation of cytochrome *c*. Like CcP, LmP reacts with $H_2O_2$ to form Compound I, which consists of a ferryl heme and a Trp radical, $Fe^{IV}$= O;$Trp^{\bullet+}$. Cytochrome *c* (Cytc) reduces the Trp radical to give Compound II, $Fe^{IV}$= O;Trp, which is followed by an intramolecular electron transfer to give $Fe^{III}$–OH;$Trp^{\bullet+}$, and in the last step, Cytc reduces the Trp radical. In this study, we have used steady-state and single-turnover kinetics to improve our understanding of the overall mechanism of LmP catalysis. While the activity of CcP greatly increases with ionic strength, the $k_{cat}$ for LmP remains relatively constant at all ionic strengths tested. Therefore, unlike CcP, where dissociation of oxidized Cytc is limiting at low ionic strengths, association/dissociation reactions are not limiting at any ionic strength in LmP. We conclude that in LmP, the intramolecular electron transfer reaction, $Fe^{IV}$= O;Trp to $Fe^{III}$–OH;$Trp^{\bullet+}$, is limiting at all ionic strengths. Unlike CcP, LmP depends on key intermolecular ion pairs to form the electron transfer competent complex. Mutating these sites causes the initial rate of association to decrease by 2 orders of magnitude and a substantial decrease in $k_{cat}$. The drop in $k_{cat}$ is due to a switch in the rate-limiting step of the mutants from intramolecular electron transfer to the rate of association in forming the LmP–LmCytc complex. These studies show that while LmP and CcP form very similar complexes and exhibit similar activities, they substantially differ in how their activity changes as a function of ionic strength. This difference is primarily due to the heavy reliance of LmP on highly specific intermolecular ion pairs, while CcP relies mainly on nonpolar interactions.

[*]**Corresponding Author:**poulos@uci.edu. Phone: (949) 824-7020.

[‖]**Present Address:** S.T.: Department of Chemistry and Biochemistry, University of California, Santa Cruz, CA 95064.

**Notes**

The authors declare no competing financial interest.

**Accession Codes**

Coordinates and structure factors have been deposited in the Protein Data Bank as entries 5AL9 and 5ALA.

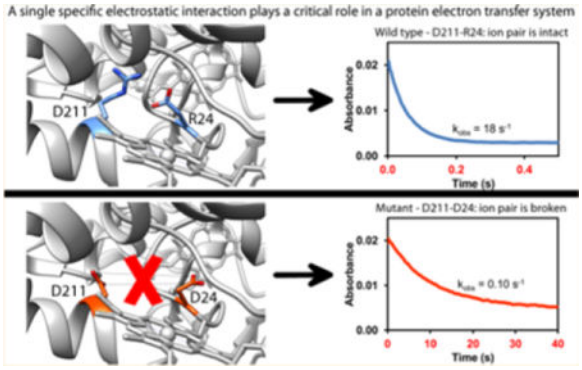


Heme peroxidases participate in a variety of physiological processes. In addition to their role in $H_2O_2$ detoxification, peroxidases play important roles in plant and fungal biosynthetic processes. Of the many plant and fungal peroxidases that have been studied, *Saccharomyces cerevisiae* cytochrome *c* peroxidase (CcP) has received special attention. CcP was the first heme peroxidase crystal structure to be determined[1] and thus has played a crucial role in furthering our understanding of structure–function relationships in heme proteins, as well as in elucidating the fundamental mechanisms of interprotein electron transfer (ET).[2] One property that has made enzymes like CcP attractive for detailed biophysical studies is that many heme peroxidases form distinct intermediates that are spectroscopically identifiable and relatively stable. This has allowed most of the intermediates in the generally accepted yeast CcP mechanism to be characterized:

$$\mathrm{CcP(Fe^{3+};Trp)+H_2O_2 \rightarrow CpdI(Fe^{4+}{=}O;Trp^{+\bullet})+H_2O} \quad (1)$$

$$\mathrm{CpdI(Fe^{4+}{=}O;Trp^{+\bullet})+yCytc(Fe^{2+}) \rightarrow CpdII(Fe^{4+}{=}O;Trp)+yCytc(Fe^{3+})} \quad (2)$$

$$\mathrm{CpdII(Fe^{4+}{=}O;Trp)+H^{+} \rightleftharpoons CpdII(Fe^{3+}-OH;Trp^{+\bullet})} \quad (3)$$

$$\mathrm{CpdII(Fe^{3+}{-}OH;Trp^{+\bullet})+yCytc(Fe^{2+})+H^{+} \rightarrow CcP(Fe^{3+};Trp)+yCytc(Fe^{3+})+H_2O} \quad (4)$$

Reaction with $H_2O_2$ gives Compound I (CpdI) (eq 1) and results in the oxidation of the ferric iron to $Fe^{IV}$ and Trp191 to a cationic radical.[3,4] In most other peroxidases, the porphyrin is oxidized rather than an amino acid side chain.[5] Previous kinetic studies[6–13] confirm that in the second step, an electron provided by the CcP redox partner, ferrocytochrome *c* (yCytc), reduces the Trp191 radical to form the second intermediate termed compound II (CpdII) (eq 2). Intramolecular ET from the Trp[14,15] reduces CcP($Fe^{IV}$=O) back to CcP($Fe^{III}$–OH), thereby re-forming the Trp radical (eq 3). In the final step, a second molecule of Cytc reduces the $Trp^{\bullet+}$ and regenerates the enzyme back to its ground state (eq 4).

For some time, yeast CcP was considered to be an outlier among peroxidases, because of the formation of the Trp radical, as well as being the only well-studied peroxidase that uses Cytc

as a reducing substrate. In large part because of the ever growing genomic databases, we now know that yeast is not unique in having a CcP, which now has been found in several other organisms. The most extensively studied non-yeast CcP is *Leishmania major* peroxidase (LmP).[16–18] Like yeast CcP, the physiological redox partner for LmP is Cytc, and LmP also forms a stable Trp radical in CpdI.[19] In addition to the crystal structures of LmP and *L. major* Cytc (LmCytc),[20] the structure of the LmP–LmCytc complex is also known[21] and is very similar to that of the yeast CcP–yCytc complex (Figure 1).

Despite the similarities between yeast CcP and LmP, there are important differences. Steady-state assays have shown that with yeast CcP, activity first increases with an increase in ionic strength, up to approximately 100–150 mM, but then decreases at higher ionic strengths,[15,22] and as we will show in this study, the LmP $k_{cat}$ is relatively insensitive to ionic strength. In addition, the steady-state kinetics of LmP are comparatively simple and most consistent with a single binding site for LmCytc, while with yeast CcP, it now is well-established that there is a second site that is populated at low ionic strengths.[15,23] Furthermore, while the complex that forms between CcP and yCytc does not have specific ionic interactions at the interface,[24] the LmP–LmCytc complex depends on specific electrostatic interactions,[21] including a key ionic interaction between LmP Asp211 and LmCytc Arg24, located at the binding interface. The role of this ion pair was initially probed by site-directed mutagenesis and steady-state Cytc oxidation assays, which revealed that replacing Arg24 with Ala increases $K_m$ by 2-fold and decreases $k_{cat}$ by 30-fold.[21] A decrease in affinity was expected, but such a large decrease in $k_{cat}$ was not, because at saturating levels of LmCytc, $k_{cat}$ might be expected to approach wild-type levels.

In this study, we have probed the intermolecular interactions in the LmP–LmCytc complex in more detail with additional mutations, steady-state kinetics, and stopped-flow spectroscopy. In addition, we establish an overall mechanism for the oxidation of LmCytc by LmP based on steady-state and single-turnover kinetics, ionic strength dependence, and mutagenesis results.

## EXPERIMENTAL PROCEDURES

### Cloning and Site-Directed Mutagenesis

The wild-type LmP construct expressed without the N-terminal hydrophobic tail as Δ34LmP was supplied by S. Adak and was cloned into the pET28a vector containing a $Kan^R$ gene and a C-terminal six-His tag as pET28a/Δ34LmP. The cytochrome *c* gene from *L. major* was expressed and purified as previously described.[20] LmP and LmCytc mutants were prepared by polymerase chain reaction (PCR) using the TaKaRa PrimeSTAR polymerase kit, and each gene was fully sequenced to ensure the fidelity of the PCR.

### Protein Expression and Purification

Expression and purification of wild-type and mutant LmP were conducted as follows. Each plasmid was transformed in *Escherichia coli* BL21(DE3) cells and plated onto LB agar with kanamycin (50 μg/mL). A single colony was used to inoculate each 5 mL of 2×YT starter culture (50 μg/mL kanamycin). The culture was incubated for 8 h at 37 °C via 220 rpm

agitation. Each liter of TB medium (50 μg/mL kanamycin) was inoculated with 2 mL of 2×YT starter culture. The cells were grown at 37 °C with 210 rpm agitation in a New Brunswick Scientific C25KC incubator until an $OD_{600}$ of 0.8 was obtained. Cells were then induced with 0.5 mM isopropyl β-D-thiogalactoside and 0.4 mM δ-aminolevulinic acid, and a new dose of kanamycin was added. Postinduction, cells were then incubated for 24 h at 25 °C and 100 rpm, after which they were harvested by centrifugation and stored at −80 °C. Cells were thawed overnight at 4 °C and resuspended by being stirred for 3 h at 4 °C in buffer A [50 mM potassium phosphate (pH 7.5), 1 mM phenylmethanesulfonyl fluoride, and 150 mM KCl]. Cells were lysed by being passed through a microfluidizer at 18K psi (Microfluidics International Co.). The soluble fraction was isolated by centrifugation at 17000 rpm and 4 °C for 1 h. The crude extract was then loaded onto a $Ni^{2+}$-nitrilotriacetate column previously equilibrated with 10 column volumes of buffer A. The column was washed with 10 column volumes of 10 mM L-histidine in buffer A before elution with a 10 to 75 mM L-histidine linear gradient in buffer A. Fractions were pooled according to an $R_z(A_{408}/A_{280}) > 1.3$, concentrated in a 10000 molecular weight cutoff (MWCO) Amicon concentrator at 4 °C, and then loaded onto a Superdex 75 column (HiLoad 16/60, GE Healthcare) controlled by an FPLC system and pre-equilibrated with buffer B [50 mM potassium phosphate (pH 7.0) and 5% glycerol]. Fractions were pooled according to the following criteria: an $R_z(A_{408}/A_{280})$ of >1.5 and spectroscopic observation of fully formed Compound I upon addition of stoichiometric amounts of hydrogen peroxide. Sample homogeneity was determined by sodium dodecyl sulfate–polyacrylamide gel electrophoresis. Expression and purification of wild-type and mutant LmCytc were previously described.[20]

## Steady-State Kinetics

All spectrophotometric steady-state activity measurements were performed at room temperature on a Cary 3E or Cary 300 UV/visible spectrophotometer. LmCytc was reduced by adding excess sodium dithionite and incubated on ice for 30 min. The dithionite was then removed when the sample was passed through an Econo-Pac 10DG desalting column (Bio-Rad) pre-equilibrated with 25 mM potassium phosphate (pH 6.5). All concentrations were determined using the appropriate molar extinction coefficients ($\varepsilon_{558}$ of 29 $mM^{-1}$ $cm^{-1}$ for reduced LmCytc, $\varepsilon_{408}$ of 113.6 $mM^{-1}$ $cm^{-1}$ for LmP, and $\varepsilon_{240}$ of 0.0436 $mM^{-1}$ $cm^{-1}$ for $H_2O_2$), and the rates of LmCytc oxidation were calculated using a $\Delta\varepsilon_{558}$ of 19.4 $mM^{-1}$ $cm^{-1}$. All activity measurements were performed in 25 mM potassium phosphate buffer (pH 6.5), and the ionic strength was increased by adding specific amounts of KCl. The reaction was initiated by the addition of $H_2O_2$ (0.18 mM), and the oxidation of ferrous LmCytc was monitored at 558 nm. All initial velocities were corrected for the enzyme-free reaction between ferrous LmCytc and $H_2O_2$, which accounted for ~15% of the enzyme-catalyzed rate. Data were fit according to the following hyperbolic term:

$$\frac{V_{max}[\mathrm{LmCytc}]}{K_{\mathrm{M}}+[\mathrm{LmCytc}]}$$

### Stopped-Flow Kinetics

All stopped-flow kinetic measurements were performed using an SX.18MV stopped-flow spectrometer (Applied Photophysics) with a dead time of ~1.0 ms and using a protocol previously established for yeast CcP.[8,10] Single-wavelength absorptions were measured using a photomultiplier detector. Ferric LmCytc was reduced and prepared with the same method used in the steady-state activity assays. CpdI was formed by adding stoichiometric amounts of $H_2O_2$, and a spectrum was recorded to ensure complete formation of CpdI. LmCytc and CpdI were loaded into separate 2.5 mL syringes and injected into the two separate drive syringes of the stopped-flow instrument. All measurements were taken in the highest ionic strength buffer used in the steady-state activity assays [25 mM potassium phosphate (pH 6.5) and 150 mM KCl]. We used a final LmCytc concentration of 0.3 $\mu$M and were able to observe at least 85% of the reaction in every experiment. Just as in the yeast CcP system, a >10-fold excess of LmP could not be used, and therefore, pseudo-first-order kinetics could not be measured. We therefore calculated the second-order rate constant $k_1$ by fitting the kinetic traces measured at 420 nm using the software provided with the stopped-flow instrument (Applied Photo-physics) and the following standard single-exponential equation:

$$A_{420}=C_1 e^{-k_{obs}t}+b$$

where $C$ is the amplitude term, $k_{obs}$ is the observed rate constant for the decay of oxidizing LmCytc, and $b$ is an offset value.

### Crystal Preparation

The LmP D211R protein sample used for crystallization was generated by thrombin digestion. A 50:1 LmP:thrombin weight ratio was used, and the sample was incubated at 25 °C for 2 h. The digested sample was then loaded onto a $Ni^{2+}$-nitrilotriacetate column previously equilibrated with buffer A and eluted with 5 mM imidazole in buffer B. The protein sample was then concentrated to 6 mg/mL in buffer B using a 10000 MWCO Amicon concentrator. Crystals were grown at room temperature in 10% (w/v) PEG MME 5000, 0.1 M MES:NaOH (pH 6.5), 7.5 mM praseodymium-(III) acetate hydrate, and 5% DMSO in a hanging drop vapor diffusion setup. Freshly grown crystals were harvested after 24 h and passed stepwise through a cryoprotectant solution containing 30% (v/v) glycerol for 4 h at 4 °C, before being flash-cooled with liquid nitrogen.

### X-ray Diffraction Data Collection, Processing, and Structure Refinement

Cryogenic (100 K) X-ray diffraction data were collected remotely at the Advanced Light Source (ALS) facility using the data collection control software *Blu-Ice*[25] and a crystal mounting robot. An ADSC Q315r CCD detector at beamlines 8.2.1 and 8.2.2 was used for data collection. Raw data frames were indexed and integrated using iMOSFLM,[26] and scaled using SCALA(AIMLESS).[27] The LmP(D211R) structure was determined by molecular replacement using Phaser[28] and the wild-type LmP structure [Protein Data Bank (PDB) entry 3RIV]. The initial difference Fourier maps were then calculated, and the models were refined using PHENIX.[29] The refined structures were validated in COOT[30]

before deposition in the RCSB Protein Data Bank. The crystallographic data collection and structure refinement statistics are summarized in Table 1 with PDB entries included.

## RESULTS

### Mechanism of CpdI Reduction in LmP

Although LmP exhibits similar Cytc oxidation rates and forms a very stable cationic Trp radical,[19] it has yet to be established if the overall mechanism is the same as in yeast CcP. We first used stopped-flow protocols established for yeast CcP[8,10] to determine if the cationic Trp radical in CpdI or $Fe^{IV}$ is reduced first by LmCytc, as it is in yeast CcP. To follow reduction of $Fe^{IV}$ in CpdI, it was first necessary to determine isosbestic points between reduced and oxidized LmCytc that could be used to follow the reduction of $Fe^{IV}$ in CpdI. The LmCytc isosbestic point at 436 nm was identified as optimal to observe a potential LmP $Fe^{IV}$ reduction. A 2-fold excess of LmP CpdI over ferrous LmCytc was used to isolate the first electron transfer step and prevent reduction of CpdII. This had to be done at a high ionic strength to observe the entire reaction within the stopped-flow instrument dead time of ~1 ms. Figure 2D shows the reaction between 0.6 $\mu$M LmP CpdI and 0.3 $\mu$M ferrous LmCytc in 25 mM potassium phosphate buffer (pH 6.5) containing 150 mM KCl. The 420 nm kinetic trace confirms that 93% of the LmCytc was oxidized during the reaction, yet the small absorbance change at 436 nm accounts for only 12%, showing that $Trp^{\bullet+}$ must have been reduced and not $Fe^{IV}$.

In an independent experiment, we measured the UV/vis spectrum of the following three mixtures incubated for 10 min at 4 °C using a 2-fold excess of LmP over LmCytc (Figure 2):

$$\mathrm{CpdI + LmCytc_{red}} \quad \text{(A)}$$

$$\mathrm{CpdI + LmCytc_{oxi}} \quad \text{(B)}$$

$$\mathrm{LmP + LmCytc_{oxi}} \quad \text{(C)}$$

While the recorded spectra of (A) and (C) do not superpose, those of (A) and (B) superpose well and have very similar features, including a heme Soret peak at the same wavelength (418 nm) and characteristic $\alpha$ and $\beta$ bands at 560 and 531 nm, respectively. These results provide spectral confirmation that the first electron transfer reduces the $Trp^{\bullet+}$ radical and not $Fe^{IV}$. Therefore, the order of electron transfer is the same as in yeast CcP.

### Mechanism of LmCytc Oxidation by LmP

The generally accepted steady-state mechanism of LmP (and yeast CcP) oxidation by Cytc is shown in Figure 3. According to previous work on CcP,[15] the off rate ($k_{-1}$ in Figure 3) should not be limiting at high ionic strengths, and the rate-limiting step is generally thought to be intramolecular ET reduction of $Fe^{IV}$ by the active site Trp to give $Fe^{III}$–OH;$Trp^{\bullet+}$ ($k_4$ in Figure 3). We probed the kinetics of the wild-type LmP system using a combination of single-turnover and steady-state kinetics (Figures 3 and 4 and Table 2). All single-turnover

stopped-flow experiments were conducted by mixing LmCytc ($Fe^{2+}$) kept at a constant concentration of 0.6 $\mu$M with changing concentrations of LmP CpdI, ranging in excess from 1.2 to 4.0 $\mu$M in a high-ionic strength buffer containing 25 mM potassium phosphate (pH 6.5) and 150 mM KCl. CpdI reduction is a second-order reaction, with a bimolecular rate constant of $2.7 \times 10^7$ $M^{-1}$ $s^{-1}$. To see whether complex formation is limiting for the wild-type (WT–WT) complex, we calculated a pseudo-first-order rate constant $k_{calc}$ of 265 $s^{-1}$ at 10 $\mu$M LmCytc, while $V_o/e$ measured from steady-state assays at 10 $\mu$M LmCytc is only 61.6 $s^{-1}$. This 5-fold difference suggests that the initial association event between LmP and LmCytc is not limiting, even at high ionic strengths. Steady-state kinetics (Table 2) show a $K_m$ increasing from 4.1 to 83 $\mu$M as the ionic strength increases, but $k_{cat}$ at saturation remains relatively unchanging, varying from 409 $s^{-1}$ at low ionic strengths to 531 $s^{-1}$ in 150 mM KCl. Compared to yeast CcP for which $k_{cat}$ increases 400-fold from low to high ionic strengths,[15] the moderate variation observed with LmP is insignificant. Overall, the insensitivity of $k_{cat}$ to increasing ionic strength suggests that the rate-limiting process is independent of ionic strength and therefore cannot be either complex association or dissociation ($k_1$ or $k_{-3}$ and $k_{-1}$ or $k_3$ in Figure 3, respectively). The rate-limiting process is also unlikely to be intermolecular ET from LmCytc $Fe^{2+}$ to the LmP Trp208 radical ($k_2$), as previous work on the CcP–Cytc system measured a very rapid ET event,[31] with a rate constant of $2 \times 10^6$ $s^{-1}$. The reason why we expect the rate to be similar in LmP is that the LmCytc heme contacts LmP at the same location as in CcP (Figure 1). Therefore, the ET pathway from the Cytc and Trp radical is the same in both LmP and CcP, and the distance between the Cytc heme and Trp radical is the same. The LmP system appears to behave like wild-type CcP at high ionic strengths, where the rate-limiting process is most likely intramolecular reduction of $Fe^{IV}$=O by Trp ($k_4$ in Figure 3). At low ionic strengths, however, the systems differ substantially, because for LmP, the rate-limiting step does not change, whereas for CcP, the rate-limiting step is generally thought to be dissociation of the complex.[15,31] To briefly summarize, the rate-limiting step in the yeast system changes from product dissociation at low ionic strengths to intramolecular ET at high ionic strengths, while for LmP, the rate-limiting step remains intramolecular ET at all ionic strengths.

## Disrupting the D211–R24 Electrostatic Interaction

Earlier, we showed that the LmCytc R24A mutant exhibited a large drop in $k_{cat}$ and a large increase in $K_m$.[21] The LmP D211R mutant exhibited similar changes in activity (Figure 4 and Table 2). These results show that either changing electrostatic complementarity at the center of the complex or disrupting a specific ion pair is responsible for the loss of activity. We also generated the LmP D211R and LmCytc R24D charge-reversal mutants. Electrostatic complementarity is maintained at the center of the complex, but simple modeling (Figure 1C) shows that the mutant Asp24 in LmCytc would not be able to form optimal H-bonding interactions with the mutant side chain Arg211 in LmP.

Furthermore, because the backbone carbonyl oxygen of the native Asp211 stabilizes binding of a $K^+$ ligand in wild-type LmP, we wanted to ensure that the metal binding site was not affected by the presence of a positively charged Arg residue replacing the native Asp. We therefore determined the X-ray crystal structure of the LmP D211R mutant to a resolution of 1.37 Å (PDB entry 5AL9), and the electron density shows either partial occupancy of the

native $K^+$ ion or full occupancy of a $Na^{2+}$ ion (Figure 5A), confirming that metal binding was preserved.

Although the mutant structure is identical to the wild-type structure, we did find one unexpected difference. The mutant crystallized in two different space groups: *C*2 with one molecule per asymmetric unit and $P2_12_12_1$ with two molecules per asymmetric unit. Diffraction data for the *C*2 form extend to 1.37 Å but only to 2.73 Å for $P2_12_12_1$. In two different crystals of the *C*2 form, we observed a very large lobe of positive difference density near the heme, consistent with a diatomic molecule covalently linked to the δ-meso carbon (Figure 5B). This is not observed in the $P2_12_12_1$ form. At present, we have no suitable explanation for what is clearly a covalently modified heme. We speculate that synchrotron radiation could possibly have reduced the iron, thus allowing an oxy complex to form, followed by further reduction to a peroxy, ultimately leading to a CpdI-like intermediate. This might generate sufficient oxidizing power to generate a heme radical that then reacts with buffer components. We observed something similar in a mutant of CcP where the distal pocket active site Trp cross-linked with an engineered Tyr residue in an iron-dependent redox process,[32] clearly indicating that redox-mediated oxidative chemistry can occur in crystals during X-ray exposure, even at cryogenic temperatures.

Kinetics of single- and double-charge-reversal mutant complexes were compared to those of the wild-type complex (Table 2). In all cases, CpdI reduction was found to be second-order, with bimolecular rate constants $k_1$ of $1.5 \times 10^5$ $M^{-1}$ $s^{-1}$ for the LmP(D211R)–LmCytc(WT) complex, $2.2 \times 10^5$ $M^{-1}$ $s^{-1}$ for the LmP(WT)–LmCytc(R24D) complex, and $2.1 \times 10^5$ $M^{-1}$ $s^{-1}$ for the double-charge-reversal mutant complex, LmP(D211R)–LmCytc(R24D), revealing an overall rate reduction of 2 orders of magnitude relative to that of the WT–WT complex.

Steady-state assays showed that all mutants were active in all combinations, but with large decreases in $k_{cat}$ and increases in $K_m$ (Table 2). Because the mutants do not saturate at high ionic strengths (Figure 4C), estimates of $K_m$ have large errors and thus are not very reliable. Because it was not possible to capture the full rate of LmCytc oxidation by stopped-flow at low ionic strengths, we focus our analysis on the high ionic strength results. For all mutants that disrupt the D211–R24 electrostatic interaction, we calculated pseudo-first-order $k_{calc}$ at a given LmCytc concentration using our measured $k_1$ from stopped-flow experiments and compared these values to $V_o/e$ measurements from steady-state kinetics (Table 3). For the D211R–R24D mutant, $k_{calc} = 2.08$ $s^{-1}$ at 10 μM LmCytc, which agrees with the value of 2.14 $s^{-1}$ obtained from steady-state kinetics. Results for the D211R–R24D mutant shows that restoring simple charge complementarity is not sufficient to recover activity. It is more likely that specific H-bonding geometry is required. Taken together, these experiments suggest that the rate of association is limiting in the mutants, at least at high ionic strengths, while as noted earlier, the rate-limiting step for the WT–WT complex is intramolecular ET from Trp208 to $Fe^{IV}$=O ($k_4$ in Figure 2).

## DISCUSSION

The results from this study show that the mechanism outlined in Figure 3 initially developed for yeast CcP[15] explains the LmP data as well. The main difference is that in yeast CcP, the rate-limiting step changes as a function of ionic strength. At low ionic strengths, the CcP–Cytc complex is so strong, dissociation of the complex becomes limiting, and a second weaker site must be taken into account.[15] At higher ionic strengths, CpdII reduction becomes limiting. With LmP, $k_{cat}$ is not very sensitive to ionic strength, strongly suggesting some process other than association or dissociation is limiting. This points to an intramolecular process, and because CpdI reduction in yeast CcP is much faster than CpdII reduction, it is very likely that $k_4$ (Figure 3) is always limiting in LmP.

Although consistent with the available data and the extensive amount of work conducted with yeast CcP, CpdII reduction is a complex process.[33] The active site Trp191 in CcP is essential for all electron transfer steps, and it is known that there is an equilibration between Trp191 and the heme iron ($k_4/k_{-4}$ in Figure 3),[34] suggesting that the electron reducing both CpdI and CpdII is transferred to $Trp^{\bullet+}$. Because ET from yCytc to $Trp^{\bullet+}$ is very fast in CpdI reduction, reduction of $Trp^{\bullet+}$ in CpdII should also be fast. It then must be the Trp-to-$Fe^{IV}$=O ET process ($k_4$ in Figure 3) that is limiting. However, because the Trp is so close to the heme iron, one might ask why would ET be so slow. Reduction of $Fe^{IV}$=O to $Fe^{III}$–OH requires protonation of the ferryl O atom and thus is a proton-coupled ET reaction, which could considerably slow the reaction. Relevant to this discussion is the fact that the $k_4/k_{-4}$ equilibrium (Figure 3) between $Fe^{IV}$=O and Trp is pH-dependent,[34] with $Fe^{IV}$=O;Trp being favored at high pH and $Fe^{III}$–OH;$Trp^{\bullet+}$ being favored at low pH, which is consistent with the requirement of ferryl O atom protonation coupled to ferryl reduction. Within the active site pocket of CcP and LmP, the distal His and Arg are obvious possible proton donors. A recent neutron diffraction study shows that the distal His52 in CcP CpdI is protonated at pH 6[35] and thus could possibly serve as the source of the required proton in the $k_4/k_{-4}$ (Figure 3) equilibrium. Also consistent with the distal His (His68 in LmP) being involved in ferryl reduction is the fact that LmP activity is highest at pH 6.5 and decreases ~2-fold at pH 8.0.[20]

This analysis and the potential role of His52 in reduction of the ferryl center are also relevant to the mechanism of CpdI formation. Because His52 is being protonated in the neutron diffraction structure, an alternative mechanism for CpdI formation has been proposed,[35] which differs substantially from the traditional view[36] that His52 shuttles a proton from the iron-linked O atom of $H_2O_2$ to the distal peroxide O atom, thus promoting heterolytic cleavage of the O–O bond. However, crystals for neutron diffraction were grown at pH 6.0, which is near the p$K_a$ of His, and the inherently stronger N–D bond should favor protonation of His52. Moreover, density functional calculations[37] indicate that the ferryl O atom carries a partial negative charge, which is expected to favor protonation of His52 in CpdI. Thus, the neutron diffraction structure is fully consistent with the generally accepted mechanism of CpdI formation[36] and its later modification to include solvent in the proton transfer process.[38]

The mutagenesis results show that LmP is far more sensitive to modification of the interface than yeast CcP. With yeast CcP, many mutants actually increase $k_{cat}$ at low ionic strengths

because some mutants increase the rate of product dissociation.[15] The most dramatic effect in yeast CcP is with charge-reversal mutants that create electrostatic clashes at the interface.[39] CcP relies more on nonpolar interactions, while LmP relies on the specific ion pairing between Asp211 in LmP and Arg24 in LmCytc. Despite such large differences, both enzymes conduct the peroxidation of Cytc at similar rates, and the structures of the complexes are remarkably similar. For detailed enzymatic studies, however, LmP offers some advantages because of the relatively simple steady-state kinetics, the simple dependence on ionic strength, and the lack of any evidence of a second LmCytc binding site. The main unknown in both systems is the intramolecular ET reaction from the active site Trp to $Fe^{IV}$=O ($k_4$ in Figure 3) that, as we discussed earlier, is most probably rate-limiting in LmP. Unfortunately, this reaction has proven to be quite difficult to study in yeast CcP. Because LmP kinetics are more straightforward, it may allow for a more detailed probing of CpdII reduction and the Trp-to-$Fe^{IV}$ ET reaction.

## Acknowledgments

We thank Dr. Irina Sevrioukova for helpful discussions and suggestions, as well as the beamline staff at Berkeley's Advanced Light Source (ALS) for their assistance during X-ray diffraction data collection.

**Funding:** This work was supported by National Institutes of Health (NIH) Grant GM57353 (T.L.P.) and NIH Training Grant GM108561 (S.A.H.).

## ABBREVIATIONS

| | |
|---|---|
| **LmP** | *L. major* peroxidase |
| **LmCytc** | *L. major* cytochrome *c* |
| **yCytc** | yeast cytochrome *c* |
| **ET** | electron transfer |
| **CcP** | yeast cytochrome *c* peroxidase |
| **CpdI** | Compound I |
| **CpdII** | Compound II |

## References

1. Poulos TL, Freer ST, Alden RA, Edwards SL, Skogland U, Takio K, Eriksson B, Xuong N, Yonetani T, Kraut J. The crystal structure of cytochrome c peroxidase. J Biol Chem. 1980; 255:575–580. [PubMed: 6243281]
2. Volkov AN, Nicholls P, Worrall JA. The complex of cytochrome c and cytochrome c peroxidase: The end of the road? Biochim Biophys Acta. 2011; 1807:1482–1503. [PubMed: 21820401]
3. Coulson AF, Yonetani T. Oxidation of cytochrome c peroxidase with hydrogen peroxide: Identification of the "endogenous donor". Biochem Biophys Res Commun. 1972; 49:391–398. [PubMed: 4344886]
4. Sivaraja M, Goodin DB, Smith M, Hoffman BM. Identification by ENDOR of Trp191 as the free-radical site in cytochrome c peroxidase compound ES. Science. 1989; 245:738–740. [PubMed: 2549632]
5. Dolphin D, Forman A, Borg DC, Fajer J, Felton RH. Compounds I of catalase and horseradish peroxidase: π-cation radicals. Proc Natl Acad Sci USA. 1971; 68:614–618. [PubMed: 5276770]

6. Geren L, Hahm S, Durham B, Millett F. Photoinduced electron transfer between cytochrome c peroxidase and yeast cytochrome c labeled at Cys 102 with (4-bromomethyl-4′-methylbipyridine) [bis(bipyridine)]ruthenium$^{2+}$ Biochemistry. 1991; 30:9450–9457. [PubMed: 1654098]
7. Hahm S, Durham B, Millett F. Photoinduced electron transfer between cytochrome c peroxidase and horse cytochrome c labeled at specific lysines with (dicarboxybipyridine)-(bisbipyridine)ruthenium(II). Biochemistry. 1992; 31:3472–3477. [PubMed: 1313296]
8. Hahm S, Geren L, Durham B, Millett F. Reaction of cytochrome c with the radical in cytochrome c peroxidase compound I. J Am Chem Soc. 1993; 115:3372–3373.
9. Roe JA, Goodin DB. Enhanced oxidation of aniline derivatives by two mutants of cytochrome c peroxidase at tryptophan 51. J Biol Chem. 1993; 268:20037–20045. [PubMed: 8397197]
10. Hahm S, Miller MA, Geren L, Kraut J, Durham B, Millett F. Reaction of horse cytochrome c with the radical and the oxyferryl heme in cytochrome c peroxidase compound I. Biochemistry. 1994; 33:1473–1480. [PubMed: 8312267]
11. Miller MA, Liu RQ, Hahm S, Geren L, Hibdon S, Kraut J, Durham B, Millett F. Interaction domain for the reaction of cytochrome c with the radical and the oxyferryl heme in cytochrome c peroxidase compound I. Biochemistry. 1994; 33:8686–8693. [PubMed: 8038158]
12. Liu RQ, Hahm S, Miller M, Durham B, Millett F. Photooxidation of Trp-191 in cytochrome c peroxidase by ruthenium-cytochrome c derivatives. Biochemistry. 1995; 34:973–983. [PubMed: 7827055]
13. Pappa HS, Tajbaksh S, Saunders AJ, Pielak GJ, Poulos TL. Probing the cytochrome c peroxidase-cytochrome c electron transfer reaction using site specific cross-linking. Biochemistry. 1996; 35:4837–4845. [PubMed: 8664274]
14. Liu RQ, Miller MA, Han GW, Hahm S, Geren L, Hibdon S, Kraut J, Durham B, Millett F. Role of methionine 230 in intramolecular electron transfer between the oxyferryl heme and tryptophan 191 in cytochrome c peroxidase compound II. Biochemistry. 1994; 33:8678–8685. [PubMed: 8038157]
15. Miller MA. A complete mechanism for steady-state oxidation of yeast cytochrome c by yeast cytochrome c peroxidase. Biochemistry. 1996; 35:15791–15799. [PubMed: 8961942]
16. Adak S, Datta AK. *Leishmania major* encodes an unusual peroxidase that is a close homologue of plant ascorbate peroxidase: A novel role of the transmembrane domain. Biochem J. 2005; 390:465–474. [PubMed: 15850459]
17. Dolai S, Yadav RK, Datta AK, Adak S. Effect of thiocyanate on the peroxidase and pseudocatalase activities of *Leishmania major* ascorbate peroxidase. Biochim Biophys Acta. 2007; 1770:247–256. [PubMed: 17118560]
18. Yadav RK, Dolai S, Pal S, Adak S. Role of tryptophan-208 residue in cytochrome c oxidation by ascorbate peroxidase from *Leishmania major*: Kinetic studies on Trp208Phe mutant and wild type enzyme. Biochim Biophys Acta. 2008; 1784:863–871. [PubMed: 18342641]
19. Jasion VS, Polanco JA, Meharenna YT, Li H, Poulos TL. Crystal structure of *Leishmania major* peroxidase and characterization of the compound I tryptophan radical. J Biol Chem. 2011; 286:24608–24615. [PubMed: 21566139]
20. Jasion VS, Poulos TL. *Leishmania major* peroxidase is a cytochrome c peroxidase. Biochemistry. 2012; 51:2453–2460. [PubMed: 22372542]
21. Jasion VS, Doukov T, Pineda SH, Li H, Poulos TL. Crystal structure of the *Leishmania major* peroxidase-cytochrome c complex. Proc Natl Acad Sci USA. 2012; 109:18390–18394. [PubMed: 23100535]
22. Kang CH, Ferguson-Miller S, Margoliash E. Steady state kinetics and binding of eukaryotic cytochromes c with yeast cytochrome c peroxidase. J Biol Chem. 1977; 252:919–926. [PubMed: 14138]
23. Mauk MR, Ferrer JC, Mauk AG. Proton linkage in formation of the cytochrome c-cytochrome c peroxidase complex: Electrostatic properties of the high- and low-affinity cytochrome binding sites on the peroxidase. Biochemistry. 1994; 33:12609–12614. [PubMed: 7918486]
24. Pelletier H, Kraut J. Crystal structure of a complex between electron transfer partners, cytochrome c peroxidase and cytochrome c. Science. 1992; 258:1748–1755. [PubMed: 1334573]

25. McPhillips TM, McPhillips SE, Chiu HJ, Cohen AE, Deacon AM, Ellis PJ, Garman E, Gonzalez A, Sauter NK, Phizackerley RP, Soltis SM, Kuhn P. Blu-Ice and the Distributed Control System: Software for data acquisition and instrument control at macromolecular crystallography beamlines. J Synchrotron Radiat. 2002; 9:401–406. [PubMed: 12409628]
26. Battye TG, Kontogiannis L, Johnson O, Powell HR, Leslie AG. iMOSFLM: A new graphical interface for diffraction-image processing with MOSFLM. Acta Crystallogr. 2011; D67:271–281.
27. Evans PR, Murshudov GN. How good are my data and what is the resolution? Acta Crystallogr. 2013; D69:1204–1214.
28. McCoy AJ, Grosse-Kunstleve RW, Adams PD, Winn MD, Storoni LC, Read RJ. Phaser crystallographic software. J Appl Crystallogr. 2007; 40:658–674. [PubMed: 19461840]
29. Adams PD, Mustyakimov M, Afonine PV, Langan P. Generalized X-ray and neutron crystallographic analysis: More accurate and complete structures for biological macromolecules. Acta Crystallogr. 2009; D65:567–573.
30. Emsley P, Cowtan K. Coot: Model-building tools for molecular graphics. Acta Crystallogr. 2004; D60:2126–2132.
31. Wang K, Mei H, Geren L, Miller MA, Saunders A, Wang X, Waldner JL, Pielak GJ, Durham B, Millett F. Design of a ruthenium-cytochrome c derivative to measure electron transfer to the radical cation and oxyferryl heme in cytochrome c peroxidase. Biochemistry. 1996; 35:15107–15119. [PubMed: 8942678]
32. Bhaskar B, Immoos CE, Shimizu H, Sulc F, Farmer PJ, Poulos TL. A novel heme and peroxide-dependent tryptophan-tyrosine cross-link in a mutant of cytochrome c peroxidase. J Mol Biol. 2003; 328:157–166. [PubMed: 12684005]
33. Mei H, Wang K, McKee S, Wang X, Waldner JL, Pielak GJ, Durham B, Millett F. Control of formation and dissociation of the high-affinity complex between cytochrome c and cytochrome c peroxidase by ionic strength and the low-affinity binding site. Biochemistry. 1996; 35:15800–15806. [PubMed: 8961943]
34. Coulson AF, Erman JE, Yonetani T. Studies on cytochrome c peroxidase. XVII Stoichiometry and mechanism of the reaction of compound ES with donors. J Biol Chem. 1971; 246:917–924. [PubMed: 5543690]
35. Casadei CM, Gumiero A, Metcalfe CL, Murphy EJ, Basran J, Concilio MG, Teixeira SC, Schrader TE, Fielding AJ, Ostermann A, Blakeley MP, Raven EL, Moody PC. Heme enzymes. Neutron cryo-crystallography captures the protonation state of ferryl heme in a peroxidase. Science. 2014; 345:193–197. [PubMed: 25013070]
36. Poulos TL, Kraut J. The stereochemistry of peroxidase catalysis. J Biol Chem. 1980; 255:8199–8205. [PubMed: 6251047]
37. Harris H, Fisher K, Dance I. Coordination and dehydrogenation of PH(3) by 23 transition metal ions in the gas phase: FTICR experiments and density functional interpretations. Inorg Chem. 2001; 40:6972–6982. [PubMed: 11754279]
38. Derat E, Shaik S, Rovira C, Vidossich P, Alfonso-Prieto M. The effect of a water molecule on the mechanism of formation of compound 0 in horseradish peroxidase. J Am Chem Soc. 2007; 129:6346–6347. [PubMed: 17472375]
39. Pearl NM, Jacobson T, Meyen C, Clementz AG, Ok EY, Choi E, Wilson K, Vitello LB, Erman JE. Effect of single-site charge-reversal mutations on the catalytic properties of yeast cytochrome c peroxidase: Evidence for a single, catalytically active, cytochrome c binding domain. Biochemistry. 2008; 47:2766–2775. [PubMed: 18232645]
40. Pettersen EF, Goddard TD, Huang CC, Couch GS, Greenblatt DM, Meng EC, Ferrin TE. UCSF Chimera: A visualization system for exploratory research and analysis. J Comput Chem. 2004; 25:1605–1612. [PubMed: 15264254]

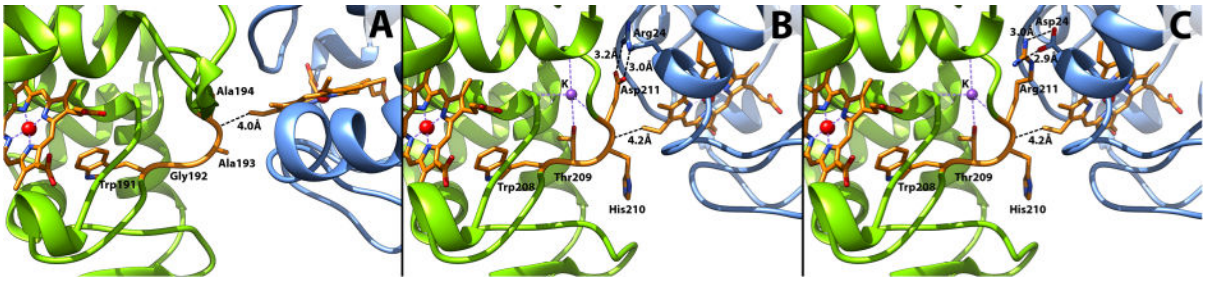


**Figure 1.**

Structures at the interface of (A) yeast CcP–Cytc, (B) Lmp–LmCytc, and (C) Lmp–LmCytc complex showing the possible orientation of the LmCytc R24D and LmP D211R mutant side chains. The section of polypeptide of the peroxidase that contacts the Cytc heme and contact distances are nearly identical in both LmP and yeast CcP. Therefore, the ET pathway and distance between the Cytc heme and Trp radical (W191 in yeast CcP and W208 in LmP) are the same. In the LmP complex, Arg24 and Asp211 form an excellent bifurcated H-bond with ideal geometry. In the charge-reversal mutant (C), Arg211 and Asp24 could be close enough for electrostatic interactions, but good hydrogen bonding geometry is not possible. Molecular graphics were made with UCSF Chimera.[40]

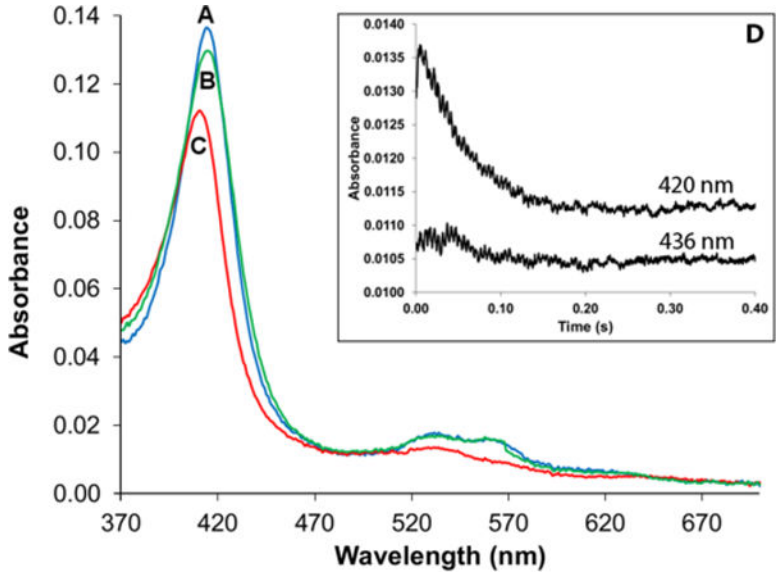


**Figure 2.**

Spectral superposition of (A) the LmP(CpdI) + reduced LmCytc reaction with (B) the CpdI + oxidized LmCytc reaction and (C) the LmP + oxidized LmCytc reaction. In each case, equimolar amounts of LmP and LmCytc were mixed in 25 mM potassium phosphate (pH 6.5) and incubated at 4 °C for 10 min before a UV/vis spectrum was recorded. (D) Stopped-flow kinetic traces monitored at 420 and 436 nm. We mixed 0.6 $\mu$M LmP(CpdI) with 0.3 $\mu$M LmCytc in a buffer containing 25 mM potassium phosphate (pH 6.5) and 150 mM KCl at 25 °C.

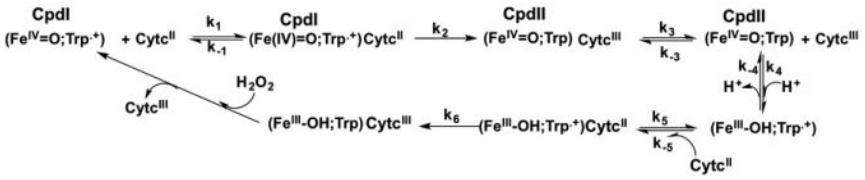


**Figure 3.**

Steady-state kinetic model of LmP catalysis adapted from ref 15.

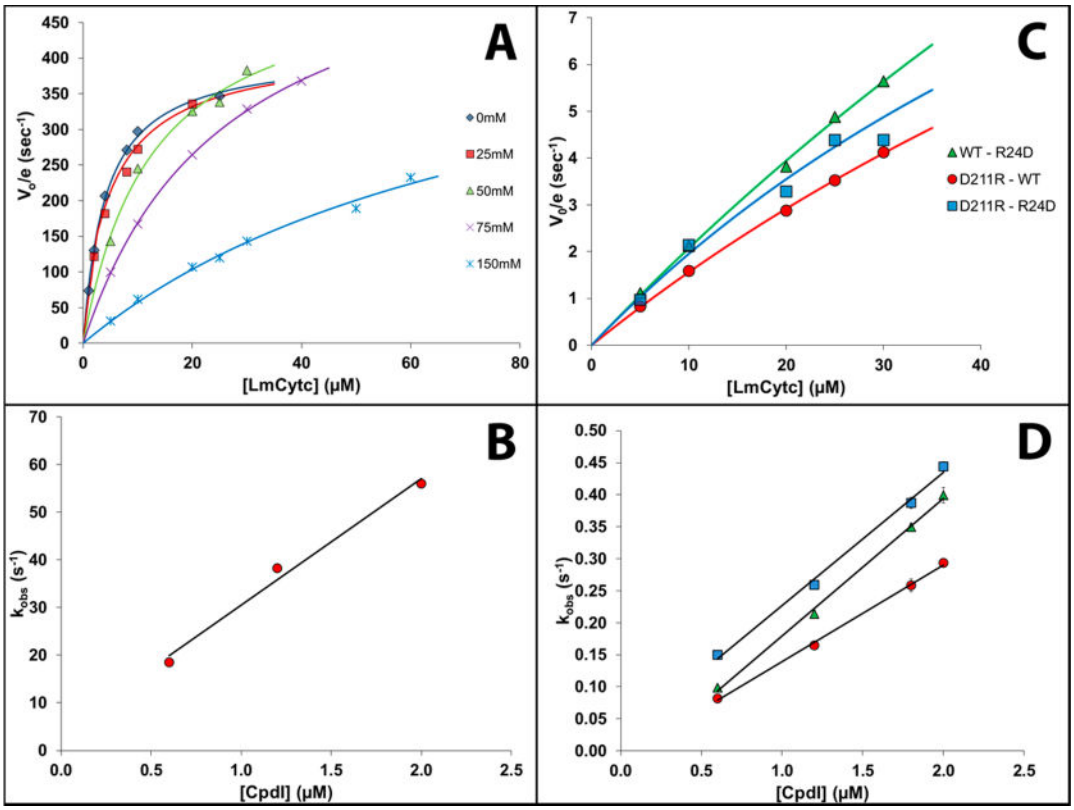


**Figure 4.**

(A) Superposed plots of $V_o/e$ vs LmCytc concentration for the wild-type complex show the effect of an increasing ionic strength. The ionic strength was increased by adding specific amounts of potassium chloride to the reaction buffer. The color scheme is as follows: blue diamonds, no KCl added; red squares, 25 mM KCl added; green triangles, 50 mM KCl added; purple crosses, 75 mM KCl added; and blue crosses, 150 mM KCl added. (B) Plot of first-order $k_{obs}$ as a function of LmP CpdI concentration obtained from single-turnover stopped-flow experiment for the wild-type complex. (C) Superposed plots of $V_o/e$ vs LmCytc concentration for the charge-reversal mutants in buffer containing 150 mM KCl. In each case, saturation was not achieved. For panels A and C, the data were fit to the Michaelis–Menten equation (see Experimental Procedures for additional details). (D) Superposed plots of first-order $k_{obs}$ as a function of LmP CpdI concentration obtained from single-turnover stopped-flow experiments for the charge-reversal mutants. For panels C and D, the color scheme is as follows: red circles, LmP(D211R)–LmCytc(WT); green triangles, LmP(WT)–LmCytc(R24D); and blue squares, LmP(D211R)–LmCytc(R24D). All stopped-flow studies were conducted in buffer containing 150 mM KCl to slow the reaction sufficiently so that only a small fraction of Cytc was oxidized in the dead time of the instrument.

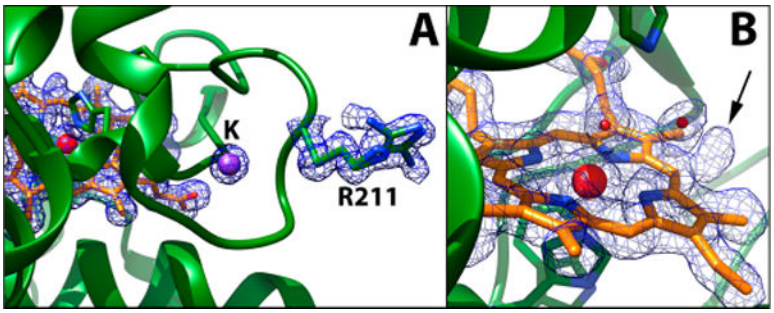


**Figure 5.**

(A) Crystal structure of the *L. major* peroxidase D211R mutant in the *C*2 space group with the $2F_o–F_c$ electron density map contoured at 1.0$\sigma$. The strong density supports binding of the metal ligand. (B) Active site heme (iron protoporphyrin IX) of *L. major* peroxidase D211R mutant with the $2F_o–F_c$ electron density map contoured at 1.0$\sigma$. The strong lobe of electron density near the $\delta$-meso carbon (indicated by the arrow) supports covalent binding of a diatomic molecule. For both panels, protein LmP is colored green and heme orange. Molecular graphics were made with UCSF Chimera.[40]

**Table 1**

Crystallographic Data and Refinement Statistics

| | | |
|---|---|---|
| PDB entry | 5AL9 | 5ALA |
| radiation source | ALS BL 8.2.1 | ALS BL 8.2.2 |
| space group | C2 | $P2_12_12_1$ |
| unit cell dimensions [*a*, *b*, *c* (Å)] | 142.44, 57.86, 36.62 | 45.88, 79.18, 179.19 |
| data resolution (highest-resolution shell) (Å) | 36.51–1.37 (1.44–1.37) | 47.71–2.73 (2.83–2.73) |
| X-ray wavelength (Å) | 1.00 | 1.00 |
| total no. of observations (highest-resolution shell) | 154623 | 71264 |
| no. of unique reflections (highest-resolution shell) | 61602 (8933) | 18116 (2365) |
| completeness (%) (highest-resolution shell) | 98.3 (98.1) | 99.9 (100) |
| $R_{merge}$ (highest-resolution shell) | 0.100 (0.898) | 0.854 (1.286) |
| $I/\sigma$ (highest-resolution shell) | 5.7 (1.5) | 18.5 (1.4) |
| $CC_{1/2}$ (highest-resolution shell) | 0.988 (0.397) | 0.752 (0.697) |
| redundancy (highest-resolution shell) | 2.5 (2.0) | 3.9 (4.1) |
| *B* factor, Wilson plot ($Å^2$) | 12.32 | 67.63 |
| no. of protein atoms | 2183 | 4349 |
| no. of heteroatoms | 77 | 153 |
| no. of waters | 278 | 80 |
| disordered residues | (A) 301–303 | (A) 301–303 (B) 301–303 |
| $R_{work}/R_{free}$ | 0.1848/0.2037 | 0.2092/0.2823 |
| root-mean-square deviation for bond lengths (Å) | 0.024 | 0.016 |
| root-mean-square deviation for bond angles (deg) | 1.12 | 1.28 |

**Table 2**

Steady-State and Single-Turnover Kinetic Parameters[a]

| | LmP(WT)–LmCytc(WT) | | | LmP(D211R)–LmCytc(WT) | | | LmP(WT)–LmCytc(R24D) | | | LmP (D211R)–LmCytc(R24D) | | |
|---|---|---|---|---|---|---|---|---|---|---|---|---|
| **added [KC1] (mM)** | $k_{cat}$ ($s^{-1}$) | $k_M$ ($\mu$M) | $k_1$ ($M^{-1}$ $s^{-1}$) | $k_{cat}$ ($s^{-1}$) | $k_M$ ($\mu$M) | $k_1$ ($M^{-1}$ $s^{-1}$) | $k_{cat}$ ($s^{-1}$) | $k_M$ ($\mu$M) | $k_1$ ($M^{-1}$ $s^{-1}$) | $k_{cat}$ ($s^{-1}$) | $k_M$ ($\mu$M) | $k_1$ ($M^{-1}$ $s^{-1}$) |
| 0 | 409 ± 9 | 4.1 ± 0.3 | | 9.1 ± 0.3 | 6.8 ± 0.7 | | 15 ± 1.0 | 11 ± 1.9 | | 11 ± 0.8 | 16 ± 2.7 | |
| 25 | 418 ± 17 | 5.3 ± 0.6 | | | | | | | | | | |
| 50 | 531 ± 35 | 13 ± 2.1 | | | | | | | | | | |
| 75 | 610 ± 10 | 26 ± 0.8 | | | | | | | | | | |
| 150 | 531 ± 74 | 83 ± 17 | $2.7 \times 10^7$ | 22 ± 2.7 | 131 ± 19 | $1.5 \times 10^5$ | 40 ± 14 | 182 ± 74 | $2.2 \times 10^5$ | 19 ± 3.9 | 89 ± 87 | $2.1 \times 10^5$ |

[a] All kinetic data were obtained in 25 mM potassium phosphate buffer (pH 6.5) at 25 °C. The ionic strength was increased by adding specific amounts of potassium chloride. Steady-state parameters were calculated by fitting the Michaelis–Menten equation where saturation occurred. See the Experimental Procedures for additional details.

**Table 3**

Comparison of Calculated Pseudo-First-Order $k_{calc}$ Values Based on Single-Turnover Data and Observed $V_o/e$ Values from Steady-State Data[a]

| | LmP(WT)–LmCytc(WT) | | LmP(D211R)–LmCytc(WT) | | LmP(WT)–LmCytc(R24D) | | LmP(D211R)–LmCytc(R24D) | |
|---|---|---|---|---|---|---|---|---|
| **[LmCytc] ($\mu$M)** | **$k_{calc}$ ($s^{-1}$)** | **$V_o/e$ ($s^{-1}$)** | **$k_{calc}$ ($s^{-1}$)** | **$V_o/e$ ($s^{-1}$)** | **$k_{calc}$ ($s^{-1}$)** | **$V_o/e$ ($s^{-1}$)** | **$k_{calc}$ ($s^{-1}$)** | **$V_o/e$ ($s^{-1}$)** |
| 5 | 133 | 31.1 ± 5.5 | 0.76 | 0.83 ± 0.13 | 1.08 | 1.11 ± 0.10 | 1.04 | 0.97 ± 0.11 |
| 10 | 265 | 61.6 ± 11 | 1.51 | 1.59 ± 0.04 | 2.15 | 2.12 ± 0.14 | 2.08 | 2.14 ± 0.05 |
| 20 | 530 | 107 ± 0.8 | 3.02 | 2.88 ± 0.16 | 4.3 | 3.82 ± 0.06 | 4.16 | 3.28 ± 0.04 |
| 25 | 663 | 120 ± 3.1 | 3.78 | 3.52 ± 0.18 | 5.38 | 4.88 ± 0.00 | 5.2 | 4.38 ± 0.42 |
| 30 | 795 | 143 ± 42 | 4.53 | 4.12 ± 0.05 | 6.45 | 5.64 ± 0.05 | 6.24 | 4.38 ± 0.02 |

[a]Values for the pseudo-first-order rate constants ($k_{calc}$) were calculated using the second-order rate constants ($k_1$) measured from the stopped-flow experiments. $V_o/e$ values were observed during the steady-state experiments. Both methods used the same buffer [25 mM potassium phosphate (pH 6.5), including an additional 150 mM KCl] and were run at 25 °C.